*Geophys. J. Int.* (2004) **157,** 1045–1060 doi: 10.1111/j.1365-246X.2004.02252.x



# Electromagnetic induction modelling based on satellite magnetic vector data

Zdeněk Martinec* and Heather McCreadie

*GeoForschungsZentrum Potsdam, Telegrafenberg,* D-14473*, Potsdam, Germany. E-mail: zdenek@hervam.troja.mff.cuni.cz*

Accepted 2004 January 28. Received 2003 January 19; in original form 2003 August 19

## SUMMARY

The first results on the modelling of magnetic signals induced by transient equatorial ring currents in the magnetosphere with a timescale of the order of days and recorded at satellite altitudes are presented. The input of modelling consists of the $X$-component of the time-series recorded by the CHAMP vector magnetometer along individual night-time, mid-latitude satellite tracks. We have not considered the magnetic signals measured along day-time tracks and above polar regions because they are disturbed by signals with sources different from magnetospheric ring currents. The modelling procedure is divided into two parts. First, the $X$-components of satellite magnetic signals are processed by a two-step least-squares analysis. As a result, the $X$-data are represented in terms of series of Legendre polynomial derivatives. Four examples of the two-step analysis of the signals recorded by the CHAMP vector magnetometer are presented. Second, forward modelling of the electromagnetic induction response of a 2-D heterogeneous conducting sphere to a transient external current excitation is carried out in the time domain using a recently developed spectral finite-element technique (Martinec *et al.* 2003), which has been modified to include satellite magnetic data. The modified approach has been verified against a semi-analytical solution for a 2-D geometry: a spherical inclusion eccentrically nested in a homogeneous sphere. The output of the forward modelling of electromagnetic induction, that is, the predicted $Z$-component at satellite altitude, can then be compared with the satellite observations to obtain data to be minimized when adjusting electrical conductivity models in future inversion modelling. To outline such a procedure, we use a 5-layer spherically symmetric model of electrical conductivity and compare the predicted and observed $Z$-data for the magnetic storm recorded by the CHAMP satellite between 2001 September 25 and 2001 October 7. The agreement between observations and predictions is quantitatively satisfactory. The main advantage of the present method is its ability to use the satellite magnetic data directly, without the need to continue them from the satellite altitude to the ground or to decompose them into the inducing and induced parts by spherical harmonic analysis.

**Key words:** 3-D electrical conductivity, electromagnetic induction, satellite magnetic data.

## 1 INTRODUCTION

The traditional approach to determining the electrical conductivity of the upper to mid mantle is based on the interpretation of land-based observatory recordings of geomagnetic time variations of external origin in the time range from several hours to several days (e.g. Eckhardt *et al.* 1963; Schultz & Larsen 1987, 1990, Banks & Ainsworth 1992). There are several problems with this approach: the global distribution of magnetic observatories is sparse and irregular; the quality of the magnetic time-series is variable; and assumptions about the spatial and time variability of external magnetic sources must often be introduced to enable electromagnetic induction modelling to be carried out (e.g. Langel & Estes 1985a). The recent high-precision magnetic missions, Ørsted and CHAMP, may have the ability to help these problems to be overcome. They provide a global coverage of high-precision vector and scalar measurements of the geomagnetic field with a significant reduction of a need to make assumptions on the spatio-temporal variability of external magnetic sources. On the other hand, however, the combined spatial and temporal character of satellite signals makes their analysis more difficult than that of their terrestrial counterparts, which

*Now at: Department of Geophysics, Faculty of Maths and Physics, Charles University, V Holesovickach 2, 180 00 Praha, Czech Republic.

 

manifest only temporal variations. Significant progress has already been made in separating the signals due to electromagnetic induction in the Earth from satellite magnetic data (Didwall 1984; Oraevsky *et al.* 1993; Olsen 1999a; Tarits & Grammatica 2000; Constable & Constable 2004; Korte *et al.* 2003).

In order to model 3-D electromagnetic induction effects in the geomagnetic field at satellite altitudes quantitatively, a transient 3-D electromagnetic induction in a heterogeneous sphere needs to be simulated. Several techniques are available to model the geomagnetic response of a 3-D heterogeneous sphere in the Fourier frequency domain, each based on a different numerical method: the spherical thin-sheet method (Fainberg & Singer 1980; Kuvshinov *et al.* 1999), finite-element method (Everett & Schultz 1996; Weiss & Everett 1998), integral-equation method (Kuvshinov *et al.* 2002), finite-difference method (Uyeshima & Schultz 2000) and spectral finite-element method (Martinec 1999). It is, however, inconvenient to study the geomagnetic induction response to a transient excitation, such as a magnetic storm, in the Fourier frequency domain. Moreover, the complicated spatial and temporal variability of satellite data favours a time-domain approach. Several time-domain methods for computing the geomagnetic induction response to a transient external source have recently been developed (Hamano 2002; Everett & Martinec 2003; Martinec *et al.* 2003).

In this paper, we will modify the existing time-domain 2-D hybrid spectral finite-element approach for electromagnetic induction modelling (Martinec *et al.* 2003) such that satellite magnetic signals are directly applied as boundary-value data at satellite altitudes. First the modified theory for implementing satellite magnetic data is presented, and the associated numerical code is verified by comparing the numerical results with a semi-analytical solution to 2-D forward modelling of transient electromagnetic induction in an axially symmetric configuration of nested spheres. Since the approach assumes that the $X$-component of the magnetic induction vector is prescribed at satellite altitudes as a series of derivatives of Legendre functions, a two-step least-squares analysis is designed to derive the expansion coefficients of this series from mid-latitude satellite data. Having excited a conducting earth by the $X$-component of the magnetic induction vector, the time-domain, spectral finite-element approach provides, among other field variables, the $Z$-component of the magnetic induction vector at satellite altitudes. We then compare this component with the CHAMP magnetic data and evaluate the acceptability of the electrical conductivity model considered.

## 2 BASIC ASSUMPTIONS ON CHAMP MAGNETIC TRACK SIGNALS

Throughout this paper, the magnetic signals induced by equatorial ring currents in the magnetosphere and measured by a satellite vector magnetometer are considered. To obtain these signals, we used the CHAMP model of the main magnetic field (Olsen 2002) and of the lithospheric magnetic field (Maus *et al.* 2002) and subtracted these static models from the CHAMP vector magnetic data. The residual magnetic time-series contain the contributions from the ionosphere and magnetosphere and their induced counterparts. We have confined ourselves to the residual magnetic time-series along night-time satellite tracks at mid-latitudes and have assumed that the contribution of ionospheric currents can be neglected. We have analysed only those periods during magnetic storms with timescales of the order of days, because the induced signal is most intense for these periods. A 25-min long magnetic signal along a night-time, mid-latitude track is considered as the instantaneous value of the residual magnetic field along the track at the time when the satellite crosses the magnetic equator. Consequently, at a given time instant, i.e. for a given night-time satellite track, an analysis of the CHAMP residual magnetic time-series can be carried out along latitude, which provides zonal spherical harmonic expansion coefficients of the data. Thus, the analysis of CHAMP magnetic data for an individual satellite track requires the assumption that the inducing and induced magnetic fields possess the axisymmetric property,

$$G^{(\mathrm{e})}_{jm}(t) = G^{(\mathrm{i})}_{jm}(t) = 0 \quad \text{for } m \neq 0, \tag{1}$$

where $G^{(\mathrm{e})}_{jm}(t)$ and $G^{(\mathrm{i})}_{jm}(t)$ are the time-dependent, spherical harmonic expansion coefficients of the external electromagnetic sources and the magnetic field generated by the induced eddy currents in the Earth, respectively.

Since the CHAMP satellite orbit is nearly polar (the inclination is approximately 87.3°), electromagnetic signals sampled along a track by the onboard magnetometer are influenced mainly by changes in the electrical conductivity of the Earth's mantle along latitude. We will not consider the effect of longitudinal variations in electrical conductivity on the signal measured along a track. That is, the electrical conductivity $\sigma$ of the Earth is assumed to be axisymmetric:

$$\sigma = \sigma(r, \vartheta) \quad \text{in } G, \tag{2}$$

where $G$ is a conducting sphere approximating a heterogeneous earth, $r$ is the radial distance from the centre of $G$, and $\vartheta$ is the colatitude.

## 3 FORMULATION OF ELECTROMAGNETIC INDUCTION FOR SATELLITE DATA

Our intention is to use the CHAMP vector magnetic data and study the response of a conducting spherical earth with an axisymmetric electrical conductivity distribution to an axisymmetric external electromagnetic excitation. This problem can be formulated mathematically as an initial boundary-value problem for the magnetic diffusion equation. Martinec (1997) solved this problem in the Fourier frequency domain by the spectral finite-element approach. Recently, Martinec *et al.* (2003) modified this approach by the implementation of a time-stepping algorithm and solved the problem in the time domain. The modified approach, called the time-domain, spectral finite-element approach, assumes that magnetic data are prescribed on the Earth's surface. For satellite measurements, this requires the continuation of magnetic data from satellite-orbit altitudes down to the Earth's surface. Since the downward continuation of satellite magnetic data poses a fundamental

problem, a modification of the time-domain, spectral finite-element approach such that satellite magnetic data can be used directly as boundary values at satellite altitudes will be given in the following sections.

Assuming an axisymmetric geometry for external sources and the conductivity model, it is convenient to formulate the initial, boundary-value problem of the global-scale electromagnetic induction in the Earth in terms of the toroidal vector potential. The classical mathematical formulation is as follows. Find the toroidal vector potential $\boldsymbol{A}$ inside the Earth $G$ such that the magnetic induction vector $\boldsymbol{B} = \text{curl}\ \boldsymbol{A}$ and

$$\left.\begin{aligned} \frac{1}{\mu}\text{curl curl}\ \boldsymbol{A} + \sigma\frac{\partial \boldsymbol{A}}{\partial t} &= \boldsymbol{0} \\ \text{div}\boldsymbol{A} &= 0 \end{aligned}\right\} \text{in } G, \tag{3}$$

$$\tag{4}$$

with the boundary condition,

$$\boldsymbol{n} \times \text{curl}\ \boldsymbol{A} = \boldsymbol{b}_0 \qquad \text{on } \partial G, \tag{5}$$

where $\mu$ is the constant permittivity of vacuum, $\boldsymbol{n}$ is the unit normal to $\partial G$, and $\boldsymbol{b}_0(\vartheta, t)$ is the tangential component of the magnetic induction vector $\boldsymbol{B}$ measured on the Earth's surface $\partial G$ at time $t \geq 0$. The mathematical assumptions on $\boldsymbol{A}$, $\sigma$ and $\boldsymbol{b}_0$ ensuring that the problem is formulated in a correct mathematical sense can be found in **K**řížek & Neittaanmäki (1990) or Martinec *et al.* (2003). Note that, owing to the assumption on the axisymmetric geometry of electrical conductivity and external sources, Ampére's law (3) does not contain the gradient of a scalar potential (e.g. section 3 in Martinec 1997).

The initial boundary-value problem (3)–(5) is formulated for ground magnetic data. In order to use satellite magnetic data without their downward continuation from satellite orbits to the Earth's surface, we extend the solution domain by the atmosphere $A$ surrounding the conducting sphere $G$. Since we consider the magnetic signals from night-time, mid-latitude tracks only, we assume that there are no electrical currents in the atmosphere $A$. This assumption is not completely correct, but it is still a good approximation (Langel & Estes 1985b). Moreover, the atmosphere $A$ is considered as a non-conducting spherical layer with the inner boundary coinciding with the surface $\partial G$ of the conducting sphere with radius $r = a$, and the outer boundary coinciding with the mean-orbit sphere $\partial A$ of radius $r = b$. The toroidal vector potential $\boldsymbol{A}_0$ in the atmosphere satisfies the following differential equations:

$$\left.\begin{aligned} \frac{1}{\mu}\text{curl curl}\ \ \boldsymbol{A}_0 &= 0 \\ \text{div}\ \boldsymbol{A}_0 &= 0 \end{aligned}\right\} \text{in } A, \tag{6}$$

$$\tag{7}$$

with the continuity condition

$$\boldsymbol{A} = \boldsymbol{A}_0 \quad \text{on } \partial G, \tag{8}$$

and the boundary condition

$$\boldsymbol{n} \times \text{curl}\ \boldsymbol{A}_0 = \boldsymbol{b}_1 \quad \text{on } \partial A, \tag{9}$$

where $\boldsymbol{b}_1$ is the is the tangential component of the magnetic induction vector $\boldsymbol{B}$ measured by a satellite magnetometer. In eqs (6) and (7), the magnetic induction vector $\boldsymbol{B}_0$ in a non-conducting atmosphere is expressed in the form $\boldsymbol{B}_0 = \text{curl}\ \boldsymbol{A}_0$ rather than in the more standard form $\boldsymbol{B}_0 = -\text{grad}\ U$, where $U$ is a magnetic scalar potential. The former expression allows the formulation of the interface condition between two solution domains in the Dirichlet form (8), while the latter expression would lead to a less convenient, namely Neumann, form of the interface condition.

In summary, the initial, boundary-value problem for the determination of the toroidal vector potential $\boldsymbol{A}$ in a conducting sphere $G$ and the toroidal vector potential $\boldsymbol{A}_0$ in a non-conducting spherical layer $A$ is governed by the partial differential equations (3) and (6) constrained by eqs (4) and (7), which are valid in $G$ and $A$, respectively, at times $t \geq 0$; by the continuity condition (8), which is applied at the interface $\partial G$; and by the boundary condition (9), which is applied at the external surface $\partial A$ at times $t \geq 0$.

## 4 WEAK FORMULATION

The initial, boundary-value problem (3)–(5) for the ground magnetic data $\boldsymbol{b}_0$ has been formulated in a weak sense by Martinec *et al.* (2003). We will modify this formulation for the case when the solution domain is extended by a non-conducting atmosphere, and magnetic data $\boldsymbol{b}_1$ are measured at satellite altitudes.

Since we intend to apply different parametrizations of the potentials $\boldsymbol{A}$ and $\boldsymbol{A}_0$, we introduce the solution spaces $V$ and $V_0$ for the conducting sphere $G$ and the non-conducting atmosphere $A$, respectively, as follows:

$$V := \{\boldsymbol{A} \,|\, \boldsymbol{A} \in L_2(G), \text{curl}\ \boldsymbol{A} \in L_2(G), \text{div}\boldsymbol{A} = 0 \text{ in } G\}, \tag{10}$$

$$V_0 := \{\boldsymbol{A}_0 | \boldsymbol{A}_0 \in C_2(A), \text{div}\boldsymbol{A}_0 = 0 \text{ in } A,\ \boldsymbol{A} = \boldsymbol{A}_0 \text{ on } \partial G\}, \tag{11}$$

where $L_2(G)$ is the space of square-integrable functions in the domain $G$, and $C_2(A)$ is the space of the functions whose derivatives up to second order are continuous in the domain $A$. Following the considerations of Martinec (1997), the weak formulation of the initial, boundary-value

problem described by eqs (3), (4), (6), (7) and (9) consists of finding the potentials $\boldsymbol{A} \in V$ and $\boldsymbol{A}_0 \in V_0$ such that, at a fixed time, they satisfy the following variational equality:

$$a(\boldsymbol{A}, \delta\boldsymbol{A}) + b(\boldsymbol{A}, \delta\boldsymbol{A}) + a_0(\boldsymbol{A}_0, \delta\boldsymbol{A}_0) = F(\boldsymbol{b}_1, \delta\boldsymbol{A}_0) \qquad \forall\delta\boldsymbol{A} \in V, \forall\delta\boldsymbol{A}_0 \in V_0. \tag{12}$$

The sesquilinear forms $a(\cdot,\cdot)$, $b(\cdot,\cdot)$, $a_0(\cdot,\cdot)$ and the functional $F(\cdot,\cdot)$ are defined as follows:

$$a(\boldsymbol{A}, \delta\boldsymbol{A}) := \frac{1}{\mu}\int_G (\mathrm{curl}\ \overline{\boldsymbol{A}} \cdot \mathrm{curl}\,\delta\boldsymbol{A})\ dV, \tag{13}$$

$$b(\boldsymbol{A}, \delta\boldsymbol{A}) := \int_G \sigma(r,\vartheta)\left(\frac{\partial\overline{\boldsymbol{A}}}{\partial t}\cdot\delta\boldsymbol{A}\right) dV, \tag{14}$$

$$a_0(\boldsymbol{A}_0, \delta\boldsymbol{A}_0) := \frac{1}{\mu}\int_A (\mathrm{curl}\ \overline{\boldsymbol{A}_0} \cdot \mathrm{curl}\,\delta\boldsymbol{A}_0)\ dV, \tag{15}$$

$$F(\boldsymbol{b}_1, \delta\boldsymbol{A}_0) := -\frac{1}{\mu}\int_{\partial A} (\overline{\boldsymbol{b}}_1 \cdot \delta\boldsymbol{A}_0)\ dS, \tag{16}$$

where $\overline{\boldsymbol{A}} = \mathrm{Re}\boldsymbol{A} - i\,\mathrm{Im}\boldsymbol{A}$ and $i = \sqrt{-1}$.

Note that the continuity condition $\boldsymbol{A} = \boldsymbol{A}_0$ on $\partial G$ can be implemented in the weak formulation in three different ways. Here, it is considered in the construction of the solution space $V_0$, see eq. (11). Alternatively, it may constrain the construction of the solution space $V$. However, the former choice is more convenient for later algebraic manipulations. The third possibility is to include this condition in the variational eq. (12) by means of the Lagrange multiplier method. Although this method is the most general way to apply a constraint to a solution, it is not used here because, as will be shown later, the continuity condition has a simple algebraic form which allows the construction of the solution space $V_0$ in a simple way.

## 5 TIME DISCRETIZATION

We approximate the partial time derivative of $\boldsymbol{A}$ in the sesquilinear form $b(\cdot,\cdot)$ by the differences of $\boldsymbol{A}$ at two subsequent time levels:

$$\frac{\partial\boldsymbol{A}}{\partial t} \approx \frac{\boldsymbol{A}(r,\vartheta,t_{i+1}) - \boldsymbol{A}(r,\vartheta,t_i)}{t_{i+1}-t_i} =: \frac{{}^{i+1}\boldsymbol{A} - {}^{i}\boldsymbol{A}}{\Delta t_i}, \tag{17}$$

where ${}^{i}\boldsymbol{A}$ denotes the values of $\boldsymbol{A}$ at discrete time levels $0 = t_0 < t_1 < \cdots < t_{i+1} < \cdots$. The variational equation (12), which is now solved at each time level $t_i$, $i = 0, 1, \ldots$, has the form

$$a({}^{i+1}\boldsymbol{A}, \delta\boldsymbol{A}) + \frac{1}{\Delta t_i} b_1\left({}^{i+1}\boldsymbol{A}, \delta\boldsymbol{A}\right) + a_0\left({}^{i+1}\boldsymbol{A}_0, \delta\boldsymbol{A}_0\right) = \frac{1}{\Delta t_i} b_1({}^{i}\boldsymbol{A}, \delta\boldsymbol{A}) + F\left({}^{i+1}\boldsymbol{b}_1, \delta\boldsymbol{A}_0\right) \quad \forall\delta\boldsymbol{A} \in V, \forall\delta\boldsymbol{A}_0 \in V_0, \tag{18}$$

where the new sesquilinear form $b_1(\cdot,\cdot)$ is defined by

$$b_1(\boldsymbol{A}, \delta\boldsymbol{A}) := \int_G \sigma(r,\vartheta)(\overline{\boldsymbol{A}}\cdot\delta\boldsymbol{A})\ dV. \tag{19}$$

The method used to discretize the variational equation (12) in time is called the implicit Euler method (**K**řížek & Neittaanmäki 1990; Press *et al.* 1992). It can be shown that this time discretization scheme is unconditionally stable. The size of the time steps $\Delta t_i$ is restricted only by the accuracy of the solution required or by the time discretization of the magnetic data $\boldsymbol{b}_1$.

## 6 SPHERICAL HARMONIC FINITE-ELEMENT PARAMETRIZATION OF A

The representation of the toroidal vector potential $\boldsymbol{A}$ and the test functions $\delta\boldsymbol{A}$ inside the conducting sphere $G$ in terms of vector spherical harmonics and finite elements is described in detail by Martinec (1997) and Martinec *et al.* (2003). Here, we only introduce the final form of the representations of $\boldsymbol{A}$ and $\delta\boldsymbol{A}$:

$$\left\{\begin{array}{c}\boldsymbol{A}(r,\vartheta,t)\\ \delta\boldsymbol{A}(r,\vartheta)\end{array}\right\} = \sum_{j=1}^{\infty}\sum_{k=1}^{\infty}\left\{\begin{array}{c}A_j^{j,k}(t)\\ \delta A_j^{j,k}\end{array}\right\}\psi_k(r)\boldsymbol{Y}_j^j(\vartheta), \tag{20}$$

where $\psi_k(r)$ are piecewise-linear finite elements on the interval $0 \le r \le a$, and $\boldsymbol{Y}_j^j(\vartheta)$ are zonal toroidal vector spherical harmonics. Their explicit forms are as follows (Varshalovich *et al.* 1989):

$$\boldsymbol{Y}_j^j(\vartheta) := -i\,P_{j1}(\cos\vartheta)\boldsymbol{e}_\varphi, \tag{21}$$

where $P_{j1}(\cos\vartheta)$ is the associated Legendre function of degree $j$ and order $m = 1$, and $\boldsymbol{e}_\varphi$ is the spherical base vector in the $\varphi$-direction. The axisymmetric geometry allows us to simplify the notation and drop the azimuthal index $m = 0$ for spherical harmonics. Note that functions

$\boldsymbol{Y}_j^j(\vartheta)$ are divergence-free, which ensures that both the toroidal vector potential $\boldsymbol{A}$ and the test functions $\delta\boldsymbol{A}$ are divergence-free. Therefore, the parametrization (20) of the potentials $\boldsymbol{A}$ and $\delta\boldsymbol{A}$ automatically satisfies the requirement on the functions from the solution space $V$ to be divergence-free.

## 7 SOLID SPHERICAL HARMONICS PARAMETRIZATION OF $A_0$

The magnetic induction vector $\boldsymbol{B}_0$ in the non-conducting atmosphere $A$ may be expressed in terms of a magnetic scalar potential as $\boldsymbol{B}_0 = -\text{grad}\, U$, where $U$ satisfies the Laplace equation. Because of the axisymmetric geometry of the inducing and induced magnetic fields, $U$ is an axisymmetric scalar and can be represented in terms of zonal scalar solid spherical harmonics $r^j Y_j(\vartheta)$ and $r^{-j-1}Y_j(\vartheta)$ as follows:

$$U(r,\vartheta,t) = a\sum_{j=1}^{\infty}\left[\left(\frac{r}{a}\right)^j G_j^{(\mathrm{e})}(t) + \left(\frac{a}{r}\right)^{j+1} G_j^{(\mathrm{i})}(t)\right] Y_j(\vartheta) \qquad \text{in } A, \tag{22}$$

where $Y_j(\vartheta)$ are zonal scalar spherical harmonics and the mean radius of the Earth, $a$, is introduced for scaling. Making use of the gradient and rotation formulae for spherical harmonics, the toroidal vector potential $\boldsymbol{A}_0$ in the non-conducting atmosphere that generates $\boldsymbol{B}_0$, that is $\boldsymbol{B}_0 = \text{curl}\,\boldsymbol{A}_0$, can be expressed as a series of zonal vector solid spherical harmonics (Martinec 1997). Thus, an unknown toroidal vector potential $\boldsymbol{A}_0$ and test functions $\delta\boldsymbol{A}_0$ can be parametrized in a non-conducting atmosphere $A$ in the form

$$\begin{Bmatrix}\boldsymbol{A}_0(r,\vartheta,t)\\ \delta\boldsymbol{A}_0(r,\vartheta)\end{Bmatrix} = ia\sum_{j=1}^{\infty}\left[\sqrt{\frac{j}{j+1}}\left(\frac{r}{a}\right)^j \begin{Bmatrix}G_j^{(\mathrm{e})}(t)\\ \delta G_j^{(\mathrm{e})}\end{Bmatrix} - \sqrt{\frac{j+1}{j}}\left(\frac{a}{r}\right)^{j+1}\begin{Bmatrix}G_j^{(\mathrm{i})}(t)\\ \delta G_j^{(\mathrm{i})}\end{Bmatrix}\right]\boldsymbol{Y}_j^j(\vartheta). \tag{23}$$

In view of this, the spherical harmonic parametrization of the sesquilinear form $a_0(\cdot,\cdot)$ defined in eq. (15) can be rearranged, after some algebraic manipulation, into the form

$$a_0(\boldsymbol{A}_0,\delta\boldsymbol{A}_0) = \frac{a^3}{\mu}\sum_{j=1}^{\infty}\left\{j\left[\left(\frac{b}{a}\right)^{2j+1}-1\right]\overline{G}_j^{(\mathrm{e})}(t)\delta G_j^{(\mathrm{e})} - (j+1)\left[\left(\frac{a}{b}\right)^{2j+1}-1\right]\overline{G}_j^{(\mathrm{i})}(t)\delta G_j^{(\mathrm{i})}\right\}, \tag{24}$$

where $a$ and $b$ are the radii of the spheres $\partial G$ and $\partial A$, respectively.

We now express the continuity condition (8), that is, $\boldsymbol{A} = \boldsymbol{A}_0$ on $\partial G$, in terms of spherical harmonics. Substituting for the spherical harmonic representation of $\boldsymbol{A}$ from eq. (20) and for $\boldsymbol{A}_0$ from eq. (23) into eq. (8) results in the constraint between the external coefficients $G_j^{(\mathrm{e})}(t)$, the internal coefficients $G_j^{(\mathrm{i})}(t)$ of the toroidal vector potential $\boldsymbol{A}_0$ in the atmosphere, and the coefficients $A_j^j(a,t)$ of the toroidal vector potential $\boldsymbol{A}$ in the Earth. This constraint is used to express the coefficients $G_j^{(\mathrm{i})}(t)$ in terms of the coefficients $G_j^{(\mathrm{e})}(t)$ and $A_j^j(a,t)$. The same procedure is applied to the test functions $\delta\boldsymbol{A}$ and $\delta\boldsymbol{A}_0$. In summary,

$$\begin{Bmatrix}G_j^{(\mathrm{i})}(t)\\ \delta G_j^{(\mathrm{i})}\end{Bmatrix} = \frac{j}{j+1}\begin{Bmatrix}G_j^{(\mathrm{e})}(t)\\ \delta G_j^{(\mathrm{e})}\end{Bmatrix} + \frac{i}{a}\sqrt{\frac{j}{j+1}}\begin{Bmatrix}A_j^j(a,t)\\ \delta A_j^j(a)\end{Bmatrix}. \tag{25}$$

The last relation enables the elimination of the coefficients $G_j^{(\mathrm{i})}(t)$ and $\delta G_j^{(\mathrm{i})}$ from the sesquilinear form $a_0(\cdot,\cdot)$:

$$\begin{aligned}a_0(\boldsymbol{A}_0,\delta\boldsymbol{A}_0) = \frac{a^3}{\mu}\sum_{j=1}^{\infty}\Bigg\{&j\left[\left(\frac{b}{a}\right)^{2j+1}-1\right]\overline{G}_j^{(\mathrm{e})}(t)\delta G_j^{(\mathrm{e})} - j\left[\left(\frac{a}{b}\right)^{2j+1}-1\right]\\ &\times\left[\frac{j}{j+1}\overline{G}_j^{(\mathrm{e})}(t)\delta G_j^{(\mathrm{e})} + \frac{i}{a}\sqrt{\frac{j}{j+1}}\overline{G}_j^{(\mathrm{e})}(t)\delta A_j^j(a) - \frac{i}{a}\sqrt{\frac{j}{j+1}}\overline{A}_j^j(a,t)\delta G_j^{(\mathrm{e})} + \frac{1}{a^2}\overline{A}_j^j(a,t)\delta A_j^j(a)\right]\Bigg\}.\end{aligned} \tag{26}$$

## 8 SPHERICAL HARMONIC PARAMETRIZATION OF SATELLITE MAGNETIC DATA

The spherical harmonic representation of magnetic data $\boldsymbol{b}_1$ at satellite altitudes can be obtained by applying the differential operator rotation on eq. (23) and substituting the result into eq. (9):

$$\boldsymbol{b}_1(b,\vartheta,t) = -i\sum_{j=1}^{\infty}\sqrt{j(j+1)}G_j^{(X)}(b,t)\boldsymbol{Y}_j^j(\vartheta), \tag{27}$$

where

$$G_j^{(X)}(b,t) := \left(\frac{b}{a}\right)^{j-1} G_j^{(\mathrm{e})}(t) + \left(\frac{a}{b}\right)^{j+2} G_j^{(\mathrm{i})}(t) \tag{28}$$

are the spherical harmonic coefficients of the $X$-component of the magnetic induction vector $\boldsymbol{B}_0$ measured at satellite altitude $r = b$, namely

$$X(b,\vartheta) := \frac{1}{r}\frac{\partial U}{\partial\vartheta}\bigg|_{r=b} = \sum_{j=1}^{\infty} G_j^{(X)}(b,t)\frac{\partial Y_j(\vartheta)}{\partial\vartheta}. \tag{29}$$

Making use of eqs (23) and (27), the functional $F(\cdot,\cdot)$ defined by eq. (16) can be expressed in the form

$$F(\boldsymbol{b}_1, \delta\boldsymbol{A}_0) = -\frac{ib^2}{\mu}\sum_{j=1}^{\infty}\sqrt{j(j+1)}G_j^{(X)}(b,t)\delta A_{0,j}^j(b), \tag{30}$$

where the spherical harmonic coefficients $\delta A_{0,j}^j(b)$ of the test functions $\delta\boldsymbol{A}_0(b,\vartheta)$ are given by eq. (23) for $r=b$:

$$\delta A_{0,j}^j(b) = ia\left[\sqrt{\frac{j}{j+1}}\left(\frac{b}{a}\right)^j \delta G_j^{(\mathrm{e})} - \sqrt{\frac{j+1}{j}}\left(\frac{a}{b}\right)^{j+1}\delta G_j^{(\mathrm{i})}\right]. \tag{31}$$

The test function coefficients $\delta G_j^{(\mathrm{i})}$ can again be eliminated from $\delta A^j{}_{0,j}(b)$ by considering the constraint (23):

$$\delta A_{0,j}^j(b) = ia\sqrt{\frac{j}{j+1}}\left[\left(\frac{b}{a}\right)^j - \left(\frac{a}{b}\right)^{j+1}\right]\delta G_j^{(\mathrm{e})} + \left(\frac{a}{b}\right)^{j+1}\delta A_j^j(a). \tag{32}$$

## 9 SPECTRAL FINITE-ELEMENT SOLUTION

Finally, we are ready to introduce the spectral finite-element solution to the initial boundary-value problem of electromagnetic induction for satellite magnetic data. The finite-dimensional functional spaces are constructed such that

$$V_h := \left\{\delta\boldsymbol{A} = \sum_{j=1}^{j_{\max}}\sum_{k=1}^{P+1}\delta A_j^{j,k}\psi_k(r)\boldsymbol{Y}_j^j(\vartheta)\right\}, \tag{33}$$

$$V_{0,h} := \left\{\delta\boldsymbol{A}_0 = \sum_{j=1}^{j_{\max}}\delta A_{0,j}^j(r)\boldsymbol{Y}_j^j(\vartheta); \delta A_{0,j}^j(r) = ia\sqrt{\frac{j}{j+1}}\left[\left(\frac{r}{a}\right)^j - \left(\frac{a}{r}\right)^{j+1}\right]\delta G_j^{(\mathrm{e})} + \left(\frac{a}{r}\right)^{j+1}\delta A_j^{j,P+1}\right\}, \tag{34}$$

where $j_{\max}$ and $P$ are finite cut-off degrees. The Galerkin method for approximating the solution of the variational equation (12) at a fixed time $t_{i+1}$ consists in finding ${}^{i+1}\boldsymbol{A}_h \in V_h$ and ${}^{i+1}\boldsymbol{A}_{0,h} \in V_{0,h}$ satisfying the equation

$$a\left({}^{i+1}\boldsymbol{A}_h, \delta\boldsymbol{A}_h\right) + \frac{1}{\Delta t_i}b_1\left({}^{i+1}\boldsymbol{A}_h, \delta\boldsymbol{A}_h\right) + a_0\left({}^{i+1}\boldsymbol{A}_{0,h}, \delta\boldsymbol{A}_{0,h}\right) = \frac{1}{\Delta t_i}b_1\left({}^{i}\boldsymbol{A}_h, \delta\boldsymbol{A}_h\right) + F\left({}^{i+1}\boldsymbol{b}_1, \delta\boldsymbol{A}_{0,h}\right)\forall\delta\boldsymbol{A}_h \in V_h, \forall\delta\boldsymbol{A}_{0,h} \in V_{0,h}. \tag{35}$$

The discrete solutions ${}^{i+1}\boldsymbol{A}_h$ and ${}^{i+1}\boldsymbol{A}_{0,h}$ of this system of equations are called the *time-domain, spectral finite-element solution*. For a given angular degree $j$ (and a fixed time $t_{i+1}$), the unknowns in eq. (35) consist of $P+1$ coefficients ${}^{i+1}A_j^{j,k}$ describing the solution in the conducting sphere $G$, and the coefficient ${}^{i+1}G_j^{(\mathrm{e})}$ describing the solution in a non-conducting spherical layer $A$. In total, there are $P+2$ unknowns in the system for a given $j$. Once this system is solved, the coefficient ${}^{i+1}G_j^{(\mathrm{i})}$ of the induced magnetic field in $A$ is computed by means of the continuity condition (25).

Inspection of eq. (30) shows that the right-hand sides of the system (35) contain the spherical harmonic expansion coefficients of the $X$-component of the magnetic induction vector $\boldsymbol{B}_0$ measured at satellite altitudes. This means that as a first step it is necessary to carry out the spherical harmonic analysis of the $X$-component of the satellite magnetic data (see Section 11). There is no need, however, to perform a spherical harmonic analysis of the $Z$-component of the satellite magnetic data. This additional analysis would enable the separation of the spherical harmonic coefficients of the external and internal magnetic fields. However, the spherical harmonic analysis of the $Z$-component of magnetic data is, in general, less reliable than the analysis of the $X$-component (Průša & Martinec 1999). This fact motivated us to design the time-domain spectral finite-element approach to the modelling of satellite magnetic data such that it avoids the requirement of carrying out a spherical harmonic analysis of the $Z$-component of the magnetic induction vector $\boldsymbol{B}_0$.

## 10 VERIFICATION

Martinec *et al.* (2003) developed the time-domain spectral finite-element method (the TISFEM method) for ground magnetic data. This method is governed by the variational equation

$$a_1\left({}^{i+1}\boldsymbol{A}_h, \delta\boldsymbol{A}_h\right) + \frac{1}{\Delta t_i}b_1\left({}^{i+1}\boldsymbol{A}_h, \delta\boldsymbol{A}_h\right) = \frac{1}{\Delta t_i}b_1\left({}^{i}\boldsymbol{A}_h, \delta\boldsymbol{A}_h\right) + F_1\left({}^{i+1}G_j^{(\mathrm{e})}, \delta\boldsymbol{A}_h\right) \quad \forall\delta\boldsymbol{A}_h \in V_h, \tag{36}$$

where the sesquilinear form $a_1(\cdot,\cdot)$ and the functional $F_1(\cdot,\cdot)$ are specified in Martinec *et al.* (2003). They tested the TISFEM method by comparison with the analytical and semi-analytical solutions to electromagnetic induction in two concentrically and eccentrically nested spheres of different but constant electrical conductivities. They also showed that the numerical code implementing the TISFEM method for ground magnetic data performs correctly, and that the TISFEM method is particularly appropriate when the external current excitation is transient. We now use this code to verify the modification of the TISFEM method for satellite magnetic data.

The complex structure of a magnetic storm will be described by a simple mathematical model that simulates the basic features of a storm. The storm ring current is considered axisymmetric with a $P_{10}(\cos\vartheta)$ spatial structure. Consequently, all spherical harmonics of the external

scalar magnetic potential are equal to zero except for the first-degree coefficient $G_1^{(e)}(t)$. After the onset of a magnetic storm at $t = 0$, the ring current quickly peaks and then decays exponentially. This time evolution is modelled by the function (Martinec *et al.* 2003)

$$G_1^{(e)}(t) = \sqrt{\frac{4\pi}{3}} A t e^{-t/\tau}, \tag{37}$$

where $\sqrt{4\pi/3}$ is the inverse norm of $P_{10}(\cos\vartheta)$, $A$ the amplitude, and $\tau$ the relaxation time describing the recovery phase of the storm. We will use $\tau = 3$ days and $A = 0.003$ nT s$^{-1}$ in the following test example.

Consider a conducting sphere $G$, consisting of two eccentrically nested spheres of which the inner sphere has a radius of 3500 km and a conductivity of 10 S m$^{-1}$, and the outer sphere $\partial G$ has a radius of $a = 6371$ km and a conductivity of 0.1 S m$^{-1}$. The inner sphere is translated along the $z$-axis by 2700 km. The radius of the mean-orbit sphere $\partial A$ is $b = a + 500$ km.

The strategy for verifying the TISFEM method for satellite magnetic data consists of three steps. First, the conducting sphere $G$ is excited by a source field with the time evolution (37) applied as the boundary-value data on the surface $\partial G$, and the numerical code implementing the TISFEM method for ground magnetic data, which is governed by the variational eq. (36), computes the electromagnetic induction response of $G$. Among other outputs, it provides the coefficients $G_j^{(i)}(t)$, $j = 1, 2, \ldots$, of the induced magnetic field. Second, the external and internal coefficients are used to generate the boundary-value data at satellite altitudes according to eq. (28). These data are applied on the mean-orbit sphere $\partial A$ and excite an electromagnetic field in the model consisting of the conducting sphere $G$ and non-conducting atmosphere $A$. The numerical code implementing the TISFEM method for satellite magnetic data, which is governed by the variational equation (35), computes the electromagnetic induction response of the model $G \oplus A$. Finally, the two methods are compared for the toroidal vector potential $\boldsymbol{A}$ and magnetic induction vector $\boldsymbol{B}$ inside the conducting sphere $G$.

In Fig. 1, the longitudinal component $A_\varphi$ of the toroidal vector potential $\boldsymbol{A}$, the radial component $B_r$, and the colatitudinal component $B_\vartheta$ of the magnetic induction vector $\boldsymbol{B}$ at the surface $\partial G$ and geomagnetic colatitude $\vartheta = 30^\circ$ are plotted as a function of time after the onset of a magnetic storm of the time history (37). In addition, the components $A_\varphi$, $B_r$ and $B_\vartheta$ at geomagnetic colatitude $\vartheta = 30^\circ$ and time $t = 15$ days are plotted as a function of the radial distance from the centre of the sphere $G$. The solution by the TISFEM method for satellite magnetic data was checked by comparing it with the solution by the TISFEM method for ground magnetic data. Fig. 1 shows that the agreement between the numerical results of the two methods is excellent.

## 11 TWO-STEP LEAST-SQUARES ANALYSIS OF SATELLITE-TRACK MAGNETIC DATA

For a given satellite night-time track, the $X$-component of signals derived from the CHAMP magnetic measurements was considered. In the first step, the main magnetic field (Olsen 2002) and the lithospheric magnetic field (Maus *et al.* 2002), both represented by the spherical harmonic series up to degree and order 65, were subtracted from the CHAMP vector magnetic measurements. The residual magnetic time-series were assumed to contain the ionospheric and magnetospheric contributions and their induced counterparts. Only the residual magnetic time-series obtained from night-time satellite tracks were considered, because the contribution of ionospheric currents can be neglected for nightsides (e.g. Olsen 1999a). The input data of the least-squares analysis are the samples of the $X$-component of the residual magnetic signal for an individual satellite track, that is, data set $(\vartheta_i, X_i)$, $i = 1, \ldots, D$, where $\vartheta_i$ is the geomagnetic colatitude of measurement side, and $D$ is the number of data points. Polar regions were excluded from the analysed series because the field due to polar currents obfuscates the equatorial ring current signals. In the following numerical examples, the magnetic data are considered at mid-latitudes within the interval from $\vartheta_1 = 40^\circ$ to $\vartheta_D = 140^\circ$. The satellite track data $(\vartheta_i, X_i)$ are referenced to the time when CHAMP passes the magnetic equator.

Consider $D$ observational equations for data $X_i$ in the form

$$\sum_{j=1}^{N} G_j^{(X)}(t) \frac{\partial Y_j(\vartheta_i)}{\partial \vartheta} + e_i = X_i, \quad i = 1, \ldots, D, \tag{38}$$

where $G_j^{(X)}(t)$ are the expansion coefficients to be determined by a least-squares analysis and $N$ is the cut-off degree. We have assumed that the measurement errors $e_i$ have zero means, uniform variances $\sigma^2$ and are uncorrelated:

$$\begin{aligned} &E e_i = 0, \\ &\text{var } e_i = \sigma^2, \\ &\text{cov}(e_i, e_j) = 0 \quad \text{for } i \neq j, \end{aligned} \tag{39}$$

where $E$, var and cov are the statistical expectancy, the variance and the covariance operator, respectively. The least-squares analysis of satellite-track magnetic measurements of the $X$-component of the magnetic induction vector is performed in two steps.

### 11.1 Change of the interval of orthogonality

In the first step, the data $X_i$ were mapped from the mid-latitude interval $\vartheta \in (\vartheta_1, \vartheta_D)$ onto the half-circle interval $\vartheta' \in (0, \pi)$ by the linear transformation

$$\vartheta' = \alpha\vartheta + \beta, \tag{40}$$

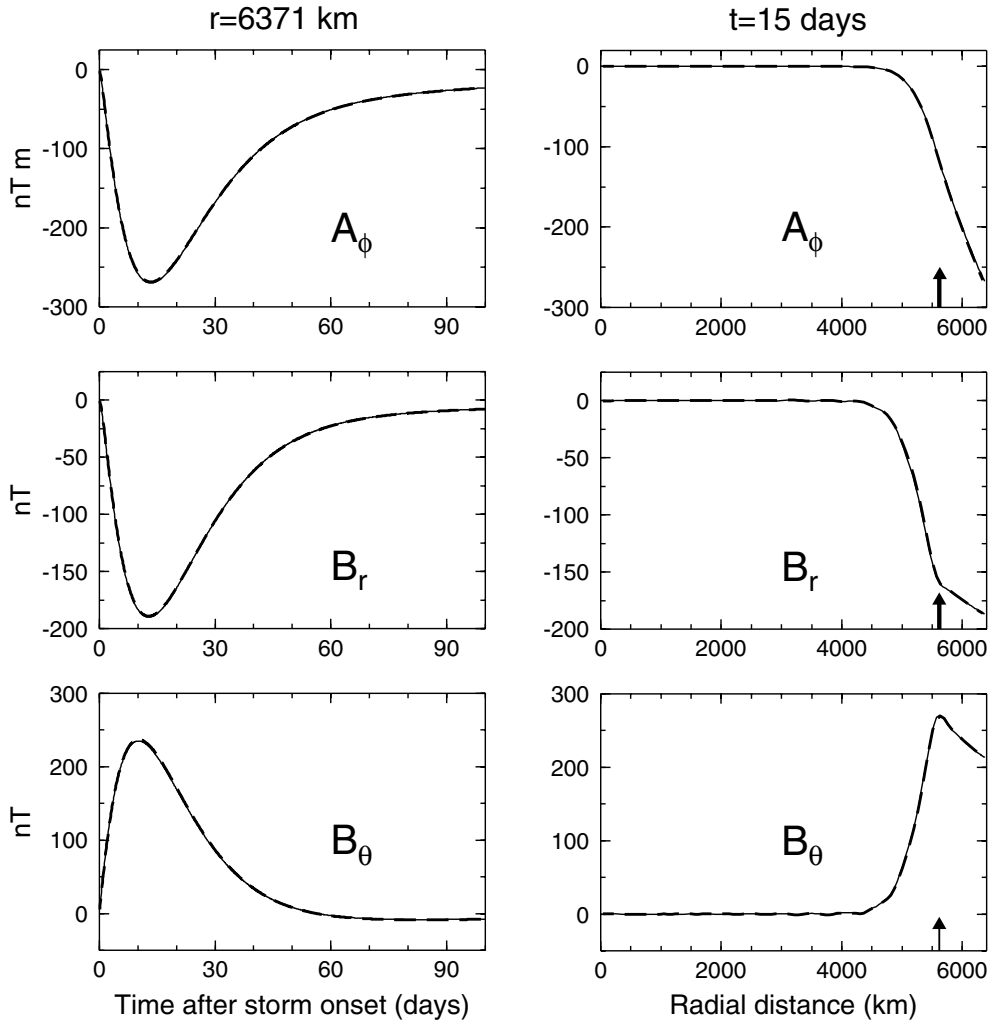


**Figure 1.** Left: surface electromagnetic induction response functions $A_\varphi(a, \vartheta, t)$ (in nT m), and $B_r(a, \vartheta, t)$ and $B_\vartheta(a, \vartheta, t)$ (in nT) of the eccentrically nested spheres model at the geomagnetic colatitude $\vartheta = 30^\circ$ as a function of time after the onset of a magnetic storm. Right: electromagnetic induction response functions $A_\varphi(r, \vartheta, t)$, $B_r(a, \vartheta, t)$ and $B_\vartheta(a, \vartheta, t)$ of the eccentrically nested spheres model at the geomagnetic colatitude $\vartheta = 30^\circ$ and the time $t = 15$ days as a function of the radial distance from the centre of the conducting sphere $G$. The response functions are computed by the TISFEM method for ground magnetic data described by eq. (37) (thick dashed lines), and by the TISFEM method for satellite magnetic data described by eq. (28) (thin solid lines). The cut-off degree of the spherical harmonic representations (33) and (34) is $j_{\max} = 40$, the number of finite elements $P = 100$, and the time step is $\Delta t = 0.1$ d. The arrows mark the position of the interface between the spherical inclusion with a radius of 3500 km and a conductivity of 10 S m$^{-1}$, translated along the $z$-axis by 2700 km, and the outer sphere with a radius of 6371 km and a conductivity of 0.1 S m$^{-1}$.

where

$$\alpha = \frac{\pi}{\vartheta_D - \vartheta_1}, \quad \beta = -\frac{\pi\vartheta_1}{\vartheta_D - \vartheta_1}, \tag{41}$$

and then adjusted by a series of Legendre polynomials:

$$X(\vartheta')\big|_{\vartheta'=\alpha\vartheta+\beta} = \sum_{j=0}^{N'} A'_j Y_j(\vartheta'), \ \vartheta' \in (0, \pi) \tag{42}$$

The expansion coefficients $A'_j$ were determined by fitting the model (42) to mid-latitude magnetic data $X_i$. Since the accuracy of CHAMP magnetic measurements is high, both long-wavelength and short-wavelength features of mid-latitude data were adjusted. That is why the cut-off degree $N'$ was chosen to be large. In the following numerical examples, $N' = 25$, while the number of data points is $D = 1550$. Because of data errors, the observational equations based on the model (42) are inconsistent and an exact solution to this system does not exist. The solution was estimated by the method of least squares. Since this method is well documented in the literature (e.g. Bevington 1969), no details are given.

### 11.2 Extrapolation of magnetic data from mid-latitudes to the half-circle

When the analysis of mid-latitude data $X_i$ is complete, the signal that best fits the mid-latitude data is extrapolated to the polar regions. The extrapolation is based on the original parametrization (38) of the $X$-component of the magnetic induction vector; thus, the requirement is

$$\sum_{j=1}^{N} G_j^{(X)}(t) \frac{\partial Y_j(\vartheta)}{\partial \vartheta}\bigg|_{\vartheta=(\vartheta'-\beta)/\alpha} \stackrel{!}{=} \sum_{k=0}^{N'} A'_k Y_k(\vartheta'), \tag{43}$$

where $A'_k$ are the coefficients determined in the previous step and $G_j^{(X)}(t)$ are now to be determined; the symbol '$\stackrel{!}{=}$' abbreviates 'it is required that'. Making use of the orthonormality property of $Y_k(\vartheta')$, the extrapolation condition (43) can be written as a system of linear algebraic equations:

$$2\pi \sum_{j=1}^{N} G_j^{(X)}(t) \int_{\vartheta'=0}^{\pi} \frac{\partial Y_j(\vartheta)}{\partial \vartheta}\bigg|_{\vartheta=(\vartheta'-\beta)/\alpha} Y_k(\vartheta') \sin\vartheta' d\vartheta' = A'_k \tag{44}$$

for $k = 0, 1, \ldots, N'$. In contrast to the previous step, only long-wavelength features of mid-latitude data were extrapolated to the polar regions; thus, $N \ll N'$. In the following numerical examples, only the range $2 \leq N \leq 6$ was considered, depending on the character of the mid-latitude data. The system of equations (44) is overdetermined, and a solution for $G_j^{(X)}(t)$ can be estimated by the method of least squares.

### 11.3 Examples of least-squares analysis of the CHAMP magnetic data

Presented here are four examples of the least-squares analysis of the CHAMP magnetic data recorded in the period from 2001 September 25 to 2001 October 7. This period was chosen because it included a magnetic storm followed by a magnetic substorm, as seen from the behaviour of the Dst index (see Fig. 2). For demonstration purposes, four CHAMP track data sets were chosen: the data recorded along track No. 6732 provides an example of data analysis before a magnetic storm occurs; track No. 6755 represents a magnetic storm reaching its main phase; track No. 6780 represents the recovery phase of a storm; and track No. 6830 represents the appearance of a substorm.

In Fig. 3, the $X$-component of the original CHAMP magnetic data reduced by the main magnetic field and the lithospheric magnetic field is shown. The top panels show the residual magnetic signals for the night-time mid-latitudes and the filtered signals after the first step of the least-squares analysis has been performed. The mid-latitude data $X_i$ are adjusted by the model (42) rather well by choosing $N' = 25$. For the sake of completeness, the second-row panels of Fig. 3 show the degree-power spectrum of the coefficients $A'_j$.

As far as the choice of the cut-off degree $N$ of coefficients $G_j^{(X)}(t)$ is concerned, we proceed as follows. We begin with degree $N = 2$, increase it by one and plot the degree-power spectrum of the coefficients $G_j^{(X)}(t)$. While the degree-power spectrum is a monotonically decreasing function of angular degree $j$, we continue increasing the cut-off degree $N$. Once the degree-power spectrum of $G_j^{(X)}(t)$ no longer decreases monotonically, the actual cut-off degree is taken from the previous step for which the degree-power spectrum was still monotonically decreasing. The degree-power spectrum of coefficients $G_j^{(X)}(t)$ for the final choice of cut-off degree $N$ is shown in the third-row panels of Fig. 3.

The criterion for choosing $N$ can be interpreted as follows. The largest energy of magnetospheric ring-current excitation is located at the angular degree $j = 1$. The leakage of the electromagnetic energy from degree $j = 1$ to higher degrees is caused by lateral heterogeneities of electrical conductivity in the Earth's mantle. The more pronounced the lateral heterogeneities, the larger the transport of energy from degree $j = 1$ to higher degrees. Accepting the criterion of a monotonically decreasing degree-power spectrum as a criterion of choosing the cut-off degree $N$, means that we regard the Earth's mantle as only weakly laterally heterogeneous.

The bottom panels of Fig. 3 show the residual signals over the whole night-time track derived from the CHAMP observations and the signals extrapolated from mid-latitude data. First, we can see the well-known fact that the original magnetic data are disturbed at the polar regions by sources other than equatorial ring currents. Second, since there is no objective criterion for evaluating the quality of the extrapolation

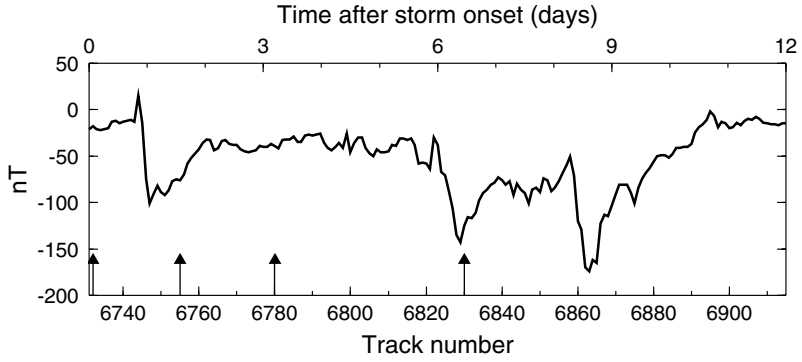


**Figure 2.** Provisional Dst index for the magnetic storm between 2001 September 25 and 2001 October 7. The arrows mark the satellite tracks chosen to demonstrate the least-squares analysis of satellite magnetic data.

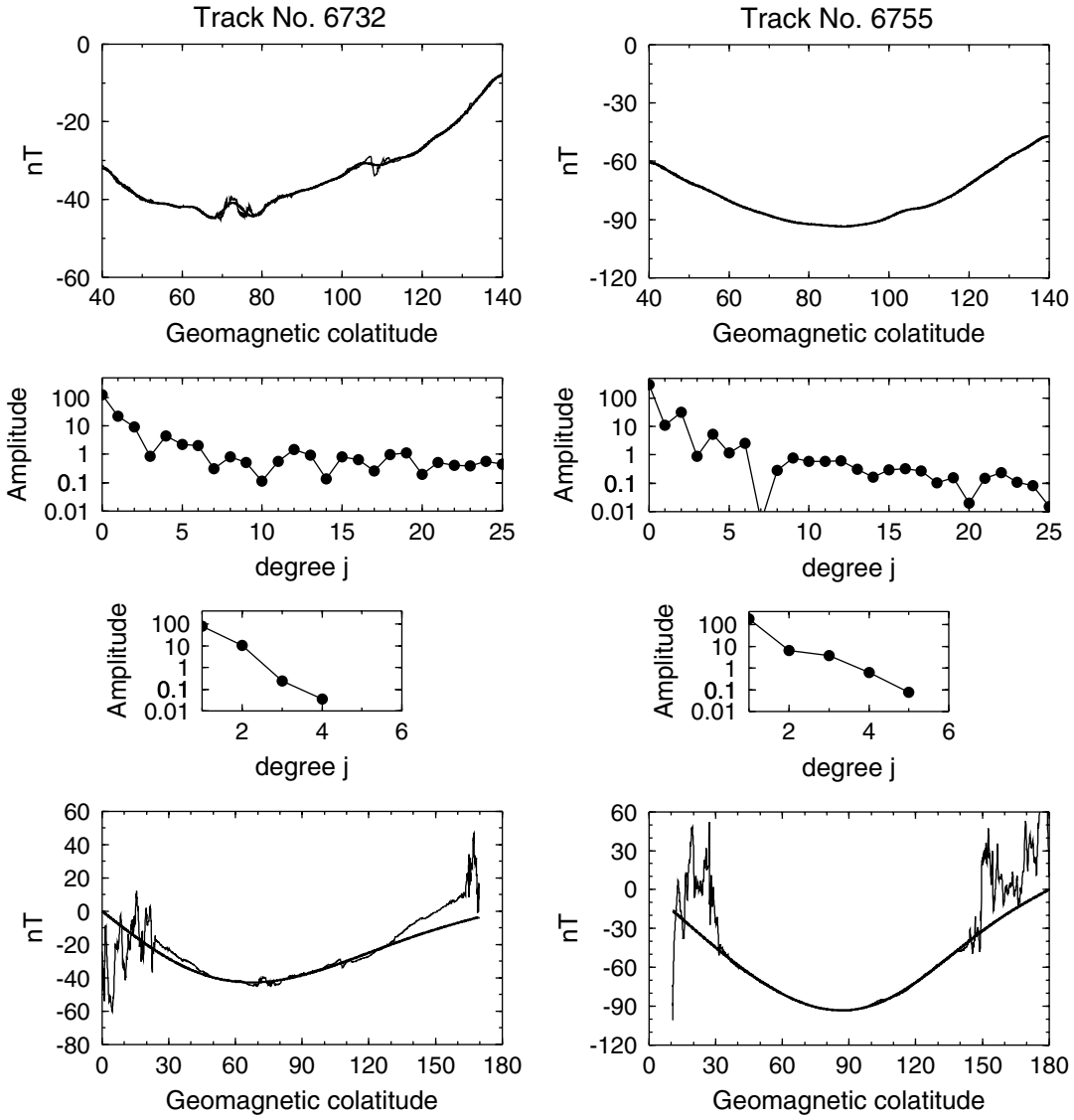


**Figure 3.** Examples of the two-step least-squares analysis of magnetic signals along four satellite tracks. The top panels show the $X$-component of the residual magnetic signals at the night-time mid-latitudes derived from the CHAMP magnetic observations (thin lines) and the predicted signals after the first step of the least-squares analysis has been completed (thick lines). The number of samples of the original signals is $D = 1550$. The second-row and third-row panels show the degree-power spectrum of the coefficients $A'_j$ and $G_j^{(X)}(t)$, respectively. The cut-off degree of the coefficients $A'_j$ is fixed to $N' = 25$, while the cut-off degree $N$ of the coefficients $G_j^{(X)}(t)$ is found by the criterion discussed in the text. The bottom panels show the $X$-component of the residual magnetic signals over the whole night-time tracks (thin lines) and the signals extrapolated from mid-latitude data according to the second step of the least-squares analysis (thick lines). As expected, both steps of the analysis represent smoothing and filtering of the original signals. The longitude when the CHAMP satellite crosses the equator of the geocentric coordinate system is $-55.19^\circ$, $127.19^\circ$, $-97.15^\circ$ and $174.23^\circ$ for track Nos 6732, 6755, 6780 and 6830, respectively.

of the $X$-component to the polar regions, it is regarded subjectively. For the track data shown here, but also for the other data for the magnetic storm considered, the extrapolation of the $X$-component from mid-latitudes to the polar regions works reasonably well provided that the cut-off degree $N$ is chosen according to the criterion we introduced.

## 12 EXAMPLE OF FORWARD ELECTROMAGNETIC INDUCTION MODELLING BASED ON THE CHAMP VECTOR DATA

After completing the least-squares analysis of magnetic data for *all* night-time, mid-latitude CHAMP tracks during the period of the magnetic storm (2001 September 25 to 2001 October 7), the time evolution of the coefficients $G_j^{(X)}(t)$ of the $X$-component of the magnetic induction vector at satellite altitude was obtained. The first panel of Fig. 4 shows the time evolution of the coefficient $G_1^{(X)}(t)$ for this period. A comparison with the Dst index for this period (Fig. 2) demonstrates the well-known fact (e.g. Olsen 1999a) that there is a high correlation between the time evolution of the Dst index and the coefficient $G_1^{(X)}(t)$. This correlation is significantly reduced for higher-degree coefficients, as shown, for instance, by the second-degree spherical harmonic coefficient $G_2^{(X)}(t)$ in Fig. 5.

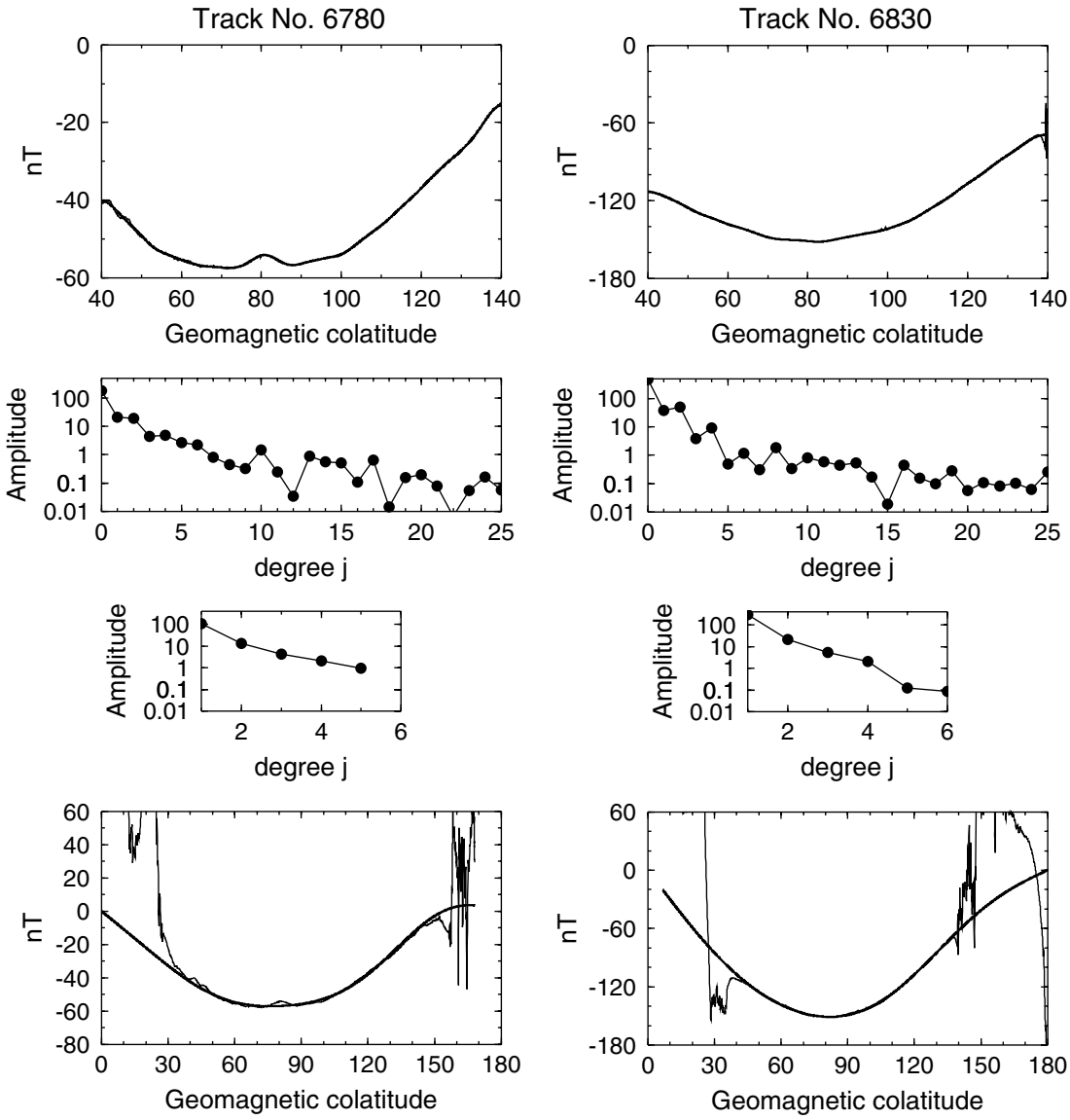


**Figure 3.** (*Continued*.)

**Table 1.** The 5-layer conductivity earth model.

| Region | Radius (km) | Conductivity (S m$^{-1}$) |
|---|---|---|
| Core | 0–3480 | 10. |
| Lower mantle | 3480–5701 | 1. |
| Upper mantle | 5701–5951 | 0.1 |
| | 5951–6301 | 0.01 |
| Lithosphere | 6301–6371 | 0.001 |

The spherical harmonic coefficients $G_j^{(X)}(t)$ were applied on the mean-orbit sphere $\partial A$ as the boundary-value data, and excite the electromagnetic field in the model consisting of the conducting sphere $G$ and the non-conducting atmosphere $A$. The geometrical parameters and the electrical conductivity of $G$ are given in Table 1. This model simplifies the results of a number of investigations on the electrical conductivity of the mantle (e.g. Pěčová *et al.* 1987; Schultz & Larsen 1987, 1990; Olsen 1999b; Xu *et al.* 2000). It is taken to demonstrate the forward modelling process. There is no particular expectation that this model will be a final global conductivity earth model.

The electromagnetic induction response of the extended model $G \oplus A$ was computed by the TISFEM method modified for the use of satellite magnetic data. There are several outputs of this method that may be used to describe the electromagnetic induction response. As a first result, the solution was specified inside the atmosphere $A$ for a point on the Earth's surface $\partial G$ from the external side, that is, for $r = a+$, and this solution was subtracted from the boundary-value data at the mean-orbit sphere $\partial A$. The difference, which corresponds to the

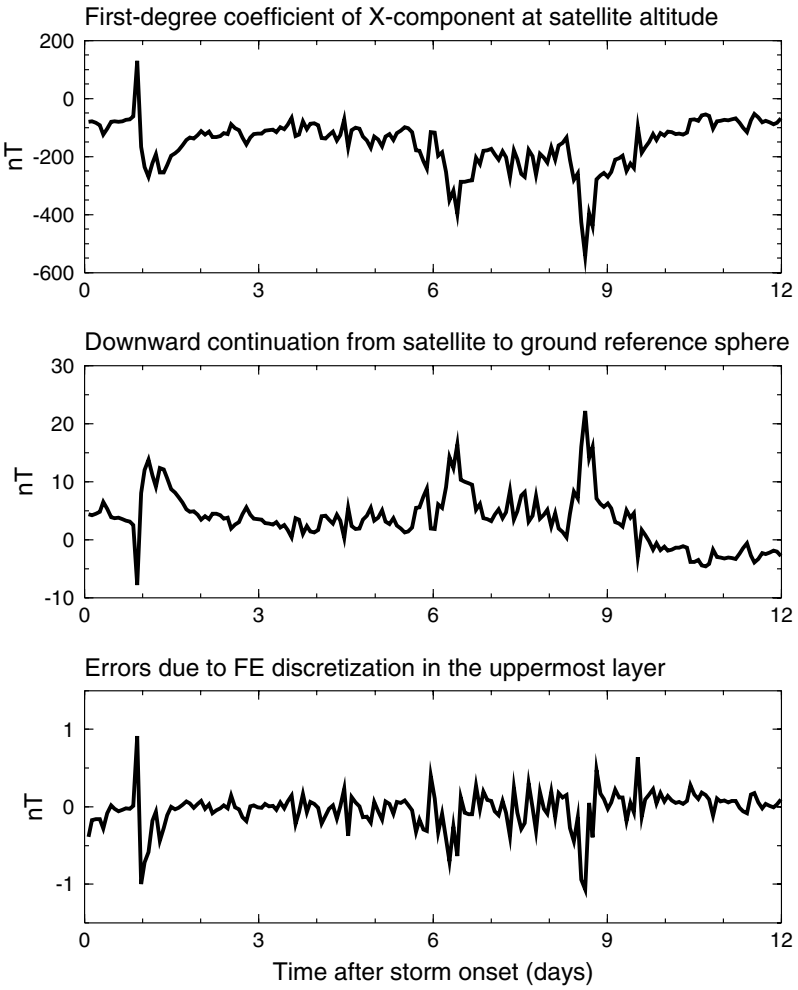


**Figure 4.** Example of forward electromagnetic induction modelling for all night-time, mid-latitude CHAMP magnetic track data over the period of the magnetic storm between 2001 September 25 and 2001 October 7. The first panel shows the time evolution of the spherical harmonic coefficient $G_1^{(X)}(t)$ for this period derived from the CHAMP magnetic observations, the second panel shows the downward continuation of $G_1^{(X)}(t)$ from the satellite altitude to the ground, and the third panel shows the jump of $G_1^{(X)}(t)$ on the Earth's surface. The results in the last two panels are based on computations performed by the TISFEM method modified for satellite magnetic data. These results are applied to the 5-layer conductivity model given in Table 1. The altitude of the CHAMP satellite above the reference geoid for the period of the magnetic storm considered is 430 km.

downward continuation of spherical harmonics of the $X$-component of the magnetic induction vector from the satellite altitude to the ground, is shown in the second panels of Figs 4 and 5 for degrees $j = 1$ and $j = 2$, respectively. It is shown that the downward continuation can reach tens of nanoteslas for degree $j = 1$ and a few nanoteslas for degree $j = 2$. For higher degrees (not shown here), the magnitude of the downward continuation of $G_j^{(X)}(t)$ does not exceed 1 nT.

The second result concerns the question of how the change in parametrization of the toroidal vector potential $\boldsymbol{A}$ inside $G$ by the spherical harmonics and linear finite elements, see eq. (20), and of the toroidal vector potential $\boldsymbol{A}_0$ inside $A$ by the solid spherical harmonics, see eq. (23), influences the continuity of the $X$-component of the magnetic induction vector $\boldsymbol{B}$ on the Earth's surface. In the third panels of Figs 4 and 5, the jump of the $X$-component of the magnetic induction vector $\boldsymbol{B}$ on the Earth's surface is plotted. A small, but non-zero, jump appears as a result of the change in parametrization of the toroidal vector potential along the radial distance at the point of the Earth's surface. Increasing the number of finite elements in the uppermost part of the conducting sphere $G$ reduces the magnitude of the jump. For instance, in Figs 4 and 5, 36 finite elements were used to parametrize $\boldsymbol{A}$ in the 70 km thick lithosphere. By a finer parametrization, with 72 finite elements, the jump in $G_1^{(X)}(t)$ is reduced from 1 nT to 0.2 nT.

Inspection of eq. (28) clarifies that the coefficients $G_j^{(X)}(t)$ are composed from a linear combination of the spherical harmonics $G_j^{(\mathrm{e})}(t)$ of the external electromagnetic sources and the spherical harmonics $G_j^{(\mathrm{i})}(t)$ of the induced magnetic field inside the Earth. There is no need to specify these coefficients separately when $G_j^{(X)}(t)$ are used as the boundary-value data for the forward modelling of the electromagnetic induction by the TISFEM method. However, as discussed after eq. (35), this approach allows the separation of the external and internal coefficients, $G_j^{(\mathrm{e})}(t)$ and $G_j^{(\mathrm{i})}(t)$, from the boundary-data coefficients, $G_j^{(X)}(t)$. In Fig. 6, the time evolution of the coefficients $G_j^{(\mathrm{e})}(t)$ and

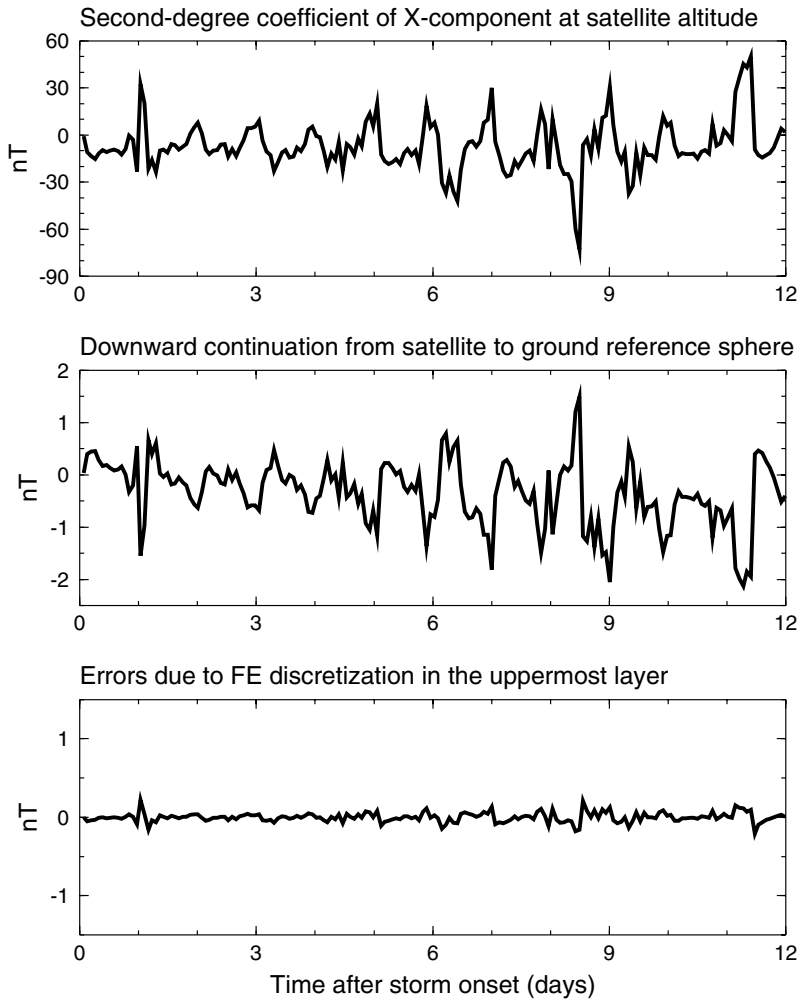


**Figure 5.** As Fig. 4, but for the second-degree coefficient $G_2^{(X)}(t)$.

$G_j^{(\mathrm{i})}(t)$, $j = 1, 2, 3$, for the period of the magnetic storm is plotted. The ratio $G_j^{(\mathrm{i})}(t)/G_j^{(\mathrm{e})}(t)$ depends on the electrical conductivity of the Earth's mantle. For the conductivity model given in Table 1, the largest ratio is for degree $j = 1$.

## 13 DISCUSSION

The TISFEM method for satellite magnetic data also allows us to model the time evolution of the $Z$-component of the magnetic induction vector on the mean-orbit sphere $\partial A$ along the satellite tracks. These predicted data can be compared with the measurements of the $Z$-component of the magnetic induction vector by the CHAMP onboard magnetometer. This comparison is plotted in Fig. 7 for the track data analysed in Fig. 3. There are differences between measured and predicted values. These differences can be used as a misfit function for the inverse electromagnetic induction modelling. Its task is to vary the conductivity structure of the Earth's mantle, such that the differences between measured and predicted values of the $Z$-component of the satellite magnetic data are minimized.

The model results shown in Fig. 7 apply to the radially symmetric earth structure given in Table 1. The procedures for the analysis of the $X$ data, and the use of them in predicting the $Z$ data for an earth conductivity model based on present generally accepted models, recreate the $Z$ data, judged by visual inspection, generally satisfactorily. However, for the tracks above the South Pacific (e.g. track No. 6830) the observed $Z$ data are always more positive then the predictions. Possible reasons for the differences between the observed and predicted $Z$ data over the Pacific region may include the exclusion of ionospheric currents from the model. The ionospheric currents in the day are well known and have wavelengths comparable with the Dst-effect currents. Little is understood about the night-time ionospheric currents. At ground level the contributions from these currents are considered insignificant, but this might not be the case at satellite altitudes. In addition, the upper mantle conductivity structure below the South Pacific may be more complex than modelled here.

## 14 CONCLUSION

The purpose of this paper has been to demonstrate the forward modelling of the electromagnetic induction in a spherical heterogeneous earth excited by transient external currents. The achievement of this paper has been to demonstrate how the values derived from the $X$-component

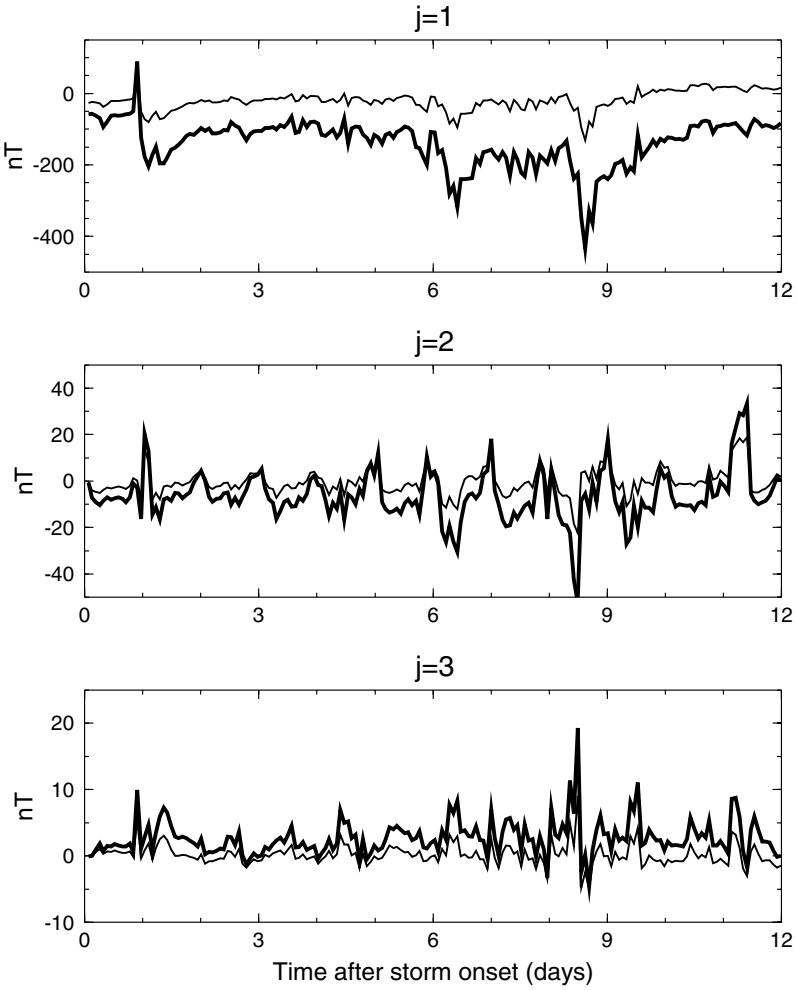


**Figure 6.** Time evolution of the coefficients $G_j^{(e)}(t)$ (thick lines) and $G_j^{(i)}(t)$ (thin lines) for degree $j = 1$ (top panel), $j = 2$ (middle panel) and $j = 3$ (bottom panel). The results apply to the magnetic storm considered in Fig. 3 and the 5-layer conductivity model given in Table 1.

data in Fig. 4 reflect the Dst index in Fig. 2, and can then be used to predict the $Z$-component data, with the agreement between prediction and observation as shown in Fig. 7. In future work, the misfits between the observed and predicted $Z$-data as in Fig. 7 (and also for all the other tracks not shown) become data to minimize, when adjusting models in an inversion process. In the present case, adjustment of the 1-D model of Table 1 might be considered, in order to obtain the best fit. In addition, the present paper has shown how a model of eccentrically nested spheres can be investigated. Further stages in interpretation will require full 3-D model capability.

The achievement of the present approach is its ability to use satellite data directly without continuing them from satellite altitude to ground level or without decomposing them into the exciting and induced parts by spherical harmonic analysis. We demonstrate this fact for a 2-D configuration, for which the electrical conductivity and the external sources of the electromagnetic variations are axisymmetrically distributed and for which the external current excitation is transient, as for a magnetic storm. The 2-D case corresponds to the situation when electromagnetic induction studies are carried out using vector magnetic data along each orbit of a satellite, such as the CHAMP satellite. The present approach can be extended to the transient electromagnetic induction in a 3-D heterogeneous sphere if the signals from multiple satellites simultaneously supplemented by ground-based magnetic observations become available in the future. Clearly, this is only the initial stage of electromagnetic induction studies based on satellite data.

## ACKNOWLEDGMENTS

We thank Detlef Wolf and two anonymous reviewers for their comments on the manuscript. This paper is a contribution to the SEAL (Sea Level Change) project, German Federal Ministry of Education and Research (BMBF) Project No. SF2000/13. The research presented in this paper was partly supported by the Grant Agency of the Czech Republic through Grant No. 205/03/1001. The provisional Dst index was provided free of charge by WDC Geomagnetism, Kyoto Dst index service. We are grateful for the support of the CHAMP geomagnetic data processing at GeoForschungsZentrum Potsdam.

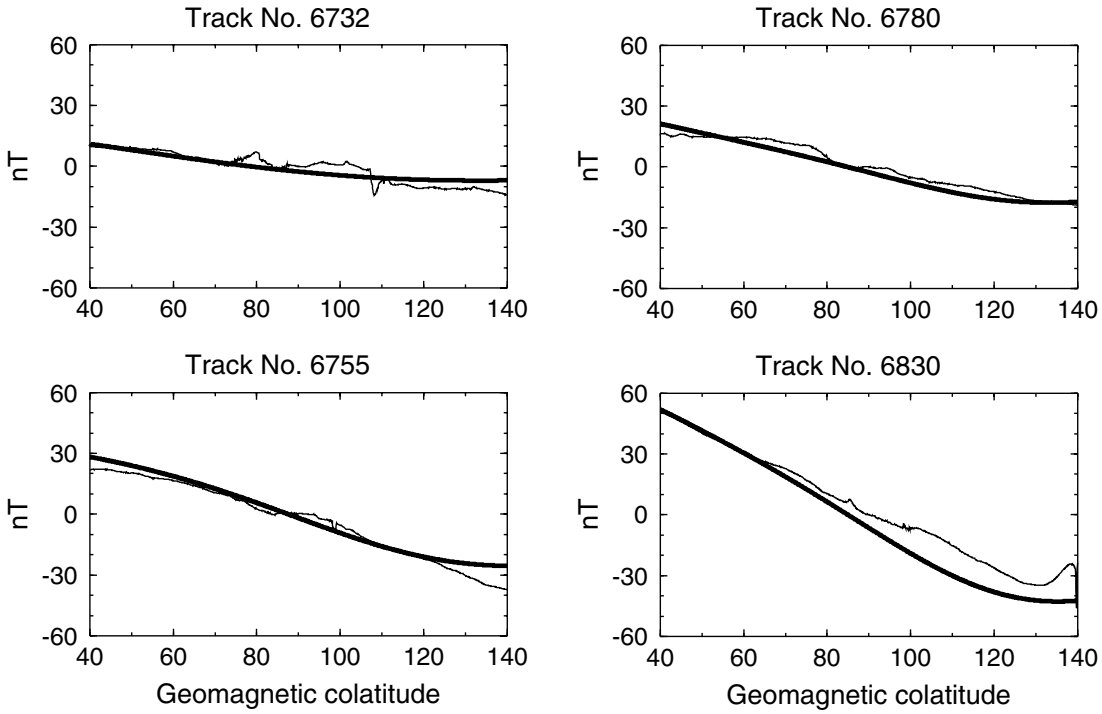


**Figure 7.** Residual magnetic signals for the *Z*-component of the magnetic induction vector derived from the CHAMP magnetic observations for the four tracks considered in Fig. 3 (thin lines), compared with the predicted counterparts computed for the conductivity model given in Table 1 (thick lines).

## REFERENCES


Banks, R.J. & Ainsworth, J.N., 1992. Global induction and the spatial structure of mid-latitude geomagnetic variations, *Geophys. J. Int.,* **110,** 251–266.

Bevington, P.R., 1969. *Data Reduction and Error Analysis for the Physical Sciences*, McGraw-Hill Book Company, New York.

Constable, S.C. & Constable, C.G., 2004. Observing geomagnetic induction in magnetic satellite measurements and associated implications for mantle conductivity, *$G^3$: Geochem., Geophys., Geosyst.,* **5,** 1–16.

Didwall, E.M., 1984. The electrical conductivity of the upper mantle as estimated from satellite magnetic field data, *J. geophys. Res.,* **89,** 537–542.

Eckhardt, D., Larner, K. & Madden, T., 1963. Long periodic magnetic fluctuations and mantle conductivity estimates, *J. geophys. Res.,* **68,** 6279–6286.

Everett, M.E. & Martinec, Z., 2003. Spatiotemporal response of a conducting sphere under simulated geomagnetic storm conditions, *Phys. Earth planet. Inter.,* **138,** 163–181.

Everett, M.E. & Schultz, A., 1996. Geomagnetic induction in a heterogeneous sphere: Azimuthally symmetric test computations and the response of an undulating 660-km discontinuity, *J. geophys. Res.,* **101,** 2765–2783.

Fainberg, E.B. & Singer, B.Sh., 1980. Electromagnetic induction in a non-uniform spherical model of the Earth, *Ann. Geophys.,* **36,** 127–134.

Hamano, Y., 2002. A new time-domain approach for the electromagnetic induction problem in a three-dimensional heterogeneous earth, *Geophys. J. Int.,* **150,** 753–769.

Korte, M., Constable, S.C. & Constable, C.G., 2003. Separation of external magnetic signal for induction studies, in, *First CHAMP Mission Results for Gravity, Magnetic and Atmospheric Studies*, pp. 315–320, eds Reigber, Ch., Lühr, H. & Schwintzer, P., Springer-Verlag Berlin.

Křížek, M. & Neittaanmäki, P., 1990. *Finite Element Approximation of Variational Problems and Applications*, Longmann Scientific and Technical, J. Wiley, New York.

Kuvshinov, A.V., Avdeev, D.B. & Pankratov, O.V., 1999. Global induction by Sq and Dst sources in the presence of oceans: bimodal solutions for non-uniform spherical surface shells above radially symmetric earth models in comparison to observations, *Geophys. J. Int.,* **137,** 630–650.

Kuvshinov, A.V., Avdeev, D.B., Pankratov, O.V., Golyshev, S.A. & Olsen, N., 2002. Modelling electromagnetic fields in a 3-D spherical earth using fast integral equation approach. In: *3D Electromagnetics*, eds Zhdanov M.S. & Wannamaker P.E., chap. 3, pp. 43–54, Elsevier, Amsterdam.

Langel, R.A. & Estes, R.H., 1985a. Large-scale, near-field magnetic fields from external sources and the corresponding induced internal field, *J. geophys. Res.,* **90,** 2487–2494.

Langel, R.A. & Estes, R.H., 1985b. The near-Earth magnetic field at 1980 determined from Magsat data, *J. geophys. Res.,* **90,** 2495–2510.

Martinec, Z., 1997. Spectral–finite element approach to two-dimensional electromagnetic induction in a spherical earth, *Geophys. J. Int.,* **130,** 583–594.

Martinec, Z., 1999. Spectral–finite element approach to three-dimensional electromagnetic induction in a spherical earth, *Geophys. J. Int.,* **136,** 229–250.

Martinec, Z., Everett, M.E. & Velímský, J., 2003. Time-domain, spectral finite-element approach to transient two-dimensional geomagnetic induction in a spherical heterogeneous earth, *Geophys. J. Int.,* **155,** 33–43.

Maus, S., Rother, M., Holme, R., Lühr, H., Olsen, N. & Haak, V., 2002. First scalar magnetic anomaly map from CHAMP satellite data indicates weak lithospheric field, *Geophys. Res. Lett.,* **29,** 10.1029/2001GL013685.

Olsen, N., 1999a. Induction studies with satellite data, *Surv. Geophys.,* **20,** 309–340.

Olsen, N., 1999b. Long-period (30 days-1 year) electromagnetic sounding and the electrical conductivity of the lower mantle beneath Europe, *Geophys. J. Int.,* **138,** 179–187.

Olsen, N., 2002. A model of the geomagnetic field and its secular variation for Epoch 2000 estimated from Ørsted data, *Geophys. J. Int.,* **149,** 453–461.

Oraevsky, V.N., Rotanova, N.M., Semenov, V. Yu, Bondar, T.N. & Abramova, D. Yu., 1993. Magnetovariational sounding of the Earth using observatory and MAGSAT satellite data., *Phys. Earth. planet. Inter.,* **78,** 119–130.

Pěčová, J., Pěč, K. & Martinec, Z., 1987. Appreciation of spherically symmetric models of electrical conductivity, *Pageoph,* **125,** 291–318.

Press, W.H., Teukolsky, S.A., Vetterling, W.T. & Flannery, B.P., 1992. *Numerical Recipes in Fortran. The Art of Scientific Computing*, Cambridge Univ. Press, Cambridge.

Průša, L. & Martinec, Z., 1999. Spherical harmonic analysis of geomagnetic variations observatory data up to degree 4 in the range of periods from 5 to 40 days, *Phys. Earth planet. Inter.,* **115,** 229–245.

Schultz, A. & Larsen, J.C., 1987. On the electrical conductivity of the mid-mantle, I, Calculation of equivalent scalar magnetotelluric response functions, *Geophys. J. R. astr. Soc.,* **88,** 733–761.

Schultz, A. & Larsen, J.C., 1990. On the electrical conductivity of the mid-mantle, II, Delineation of heterogeneity by application of extremal inverse solutions, *Geophys. J. Int.,* **101,** 565–580.

Tarits, P. & Grammatica, N., 2000. Electromagnetic induction effects by the solar quiet magnetic field at satellite altitude, *Geophys. Res. Lett.,* **27,** 4009–4012.

Varshalovich, D.A., Moskalev, A.N. & Khersonskii, V.K., 1989. *Quantum Theory of Angular Momentum,* World Scientific Publ., Singapore.

Uyeshima, M. & Schultz, A., 2000. Geoelectromagnetic induction in a heterogeneous sphere: a new three-dimensional forward solver using a conservative staggered-grid finite difference method, *Geophys. J. Int.,* **140,** 636–650.

Weiss, C.J. & Everett, M.E., 1998. Geomagnetic induction in a heterogeneous sphere: fully three-dimensional test computations and the response of a realistic distribution of oceans and continents, *Geophys. J. Int.,* **135,** 650–662.

Xu, Y., Shankland, T.J. & Poe, B.T., 2000. Laboratory-based electrical conductivity in the Earth's mantle, *J. geophys. Res.,* **105,** 27 865–27 875.